Strength of polycrystalline coarse-grained platinum to 330 GPa and of nanocrystalline platinum to 70 GPa from high-pressure x-ray diffraction data

Anil K. Singh,[1,a)] Hanns-Peter Liermann,[2] Yuichi Akahama,[3] Surendra K. Saxena,[4] and Eduardo Menéndez-Proupin[5]
[1]*Materials Science Division, National Aerospace Laboratories, Bangalore 560017, India*
[2]*HPCAT and Geophysical Laboratory, Carnegie Institution of Washington, 9700 Cass Ave., Bldg. 434, Argonne IL 60439, USA*
[3]*Graduate School of Material Science, University of Hyogo, 3-2-1, Kouto, Kamigohri, Hyogo 678-1297, Japan*
[4]*Center for the Study of Matter at Extreme Conditions (CeSMEC), Florida International University, Miami, Florida 33199, USA*
[5]*Department of Physics, Faculty of Science, University of Chile, P.O. Box 653, Santiago, Chile*

X-ray diffraction patterns from platinum foil (~300 nm grain size) have been recorded up to 330 GPa using a beveled-anvil diamond cell. The compressive strength has been determined from the analysis of the diffraction linewidths. In a separate set of experiments, coarse-grained platinum powder (~300 nm grain size) is compressed up to 64 GPa in a diamond anvil cell with 300 μm flat-face anvils and diffraction patterns are recorded. The strengths as functions of pressure derived in the two sets of experiments agree well. The strength increases linearly from 0.21(2) GPa at zero pressure to 9.8(4) GPa at a pressure of 330 GPa. The nanocrystalline platinum sample (~20 nm average grain size) exhibits much higher strength and increases linearly from 3.0(1) to 8.0(3) GPa as the pressure is increased from zero pressure to 70 GPa. The grain size of nanocrystalline sample decreases with increasing pressure. The effect of nonhydrostatic compression on the pressures determined with platinum as a pressure marker in high-pressure x-ray diffraction studies is discussed.

I. INTRODUCTION

Elemental platinum is used as a pressure marker in high-pressure x-ray diffraction experiments[1–4] with diamond anvil cells (DACs) because of the stability of the ambient pressure face-centered-cubic phase to high pressures, high scattering power for x rays, chemical inertness, and well established equation of state.[5–9] Furthermore, its ability to absorb infrared radiation makes it a good absorber in the laser-heated experiments. In addition to a reliable pressure standard, the acquisition of high-precision diffraction data requires hydrostatic pressure condition in sample chamber. The use of helium pressure transmitting medium can provide near-hydrostatic pressures to ~60 GPa. At higher pressures, the stiffening of the pressure transmitting medium and the sample (marker) bridging the anvils are the factors that lead to nonhydrostatic pressures. The pressures in the range of a few hundred gigapascals are inevitably nonhydrostatic. The nonhydrostatic compression effects cause the pressure-volume relation to deviate from the correct one[10–15] and the compressive strengths of both the sample and pressure marker determine the magnitude of the deviation. In this respect, the strength of Pt as a function of pressure is an important parameter. The strength of Pt has been reported earlier to 24 GPa.[16] It is important to extend the upper pressure limit of measurement, since Pt is used as a marker to much higher pressures. The Pt samples used as pressure markers are often in the form of fine powder. Following the trend seen in earlier studies,[17–19] the high-pressure strength of Pt is expected to depend on the grain size. In this article, we report the strength of polycrystalline Pt samples of two different grain sizes. The coarse-grained Pt has been studied to 330 GPa and nanocrystalline Pt to 70 GPa.

The solid sample, when compressed between the anvils of a DAC, flows radially and equilibrium is reached when the frictional forces between the sample-anvil interfaces balance the forces causing the flow. It is convenient to consider the equilibrium stress state in the sample as a superposition of two types of stresses, macrostresses and microstresses.[20] The macrostresses represent average stresses in a direction that cuts across large number of crystallites in the sample. These stresses produce strains that cause the diffraction lines to shift. We consider the stress state at the center of sample. As the macrostresses are axially symmetric about the load axis of the DAC that passes through the center of the sample, the stress state is completely described by three principal stresses, σ_3 along the symmetry axis and two equal stresses σ_1 in the plane parallel to the anvil face. The difference $(\sigma_3-\sigma_1)$ equals the yield strength at a pressure $(2\sigma_1+\sigma_3)/3$.[21] The equations based on the lattice strain theory[11–13,22–25] have been used to analyze the high-pressure x-ray diffraction patterns from polycrystalline samples and information on the mechanical properties such as yield strength[14–16,26–32] and elasticity[33–45] has been obtained. The

a)Author to whom correspondence should be addressed. Electronic mail: aksingh@css.nal.res.in.

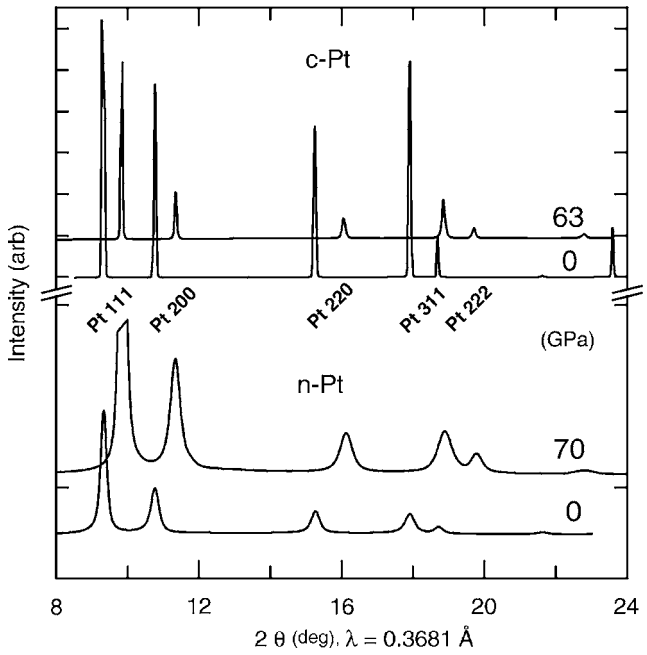

FIG. 1. X-ray diffraction patterns of *c*-Pt-A and *n*-Pt recorded at HPCAT.

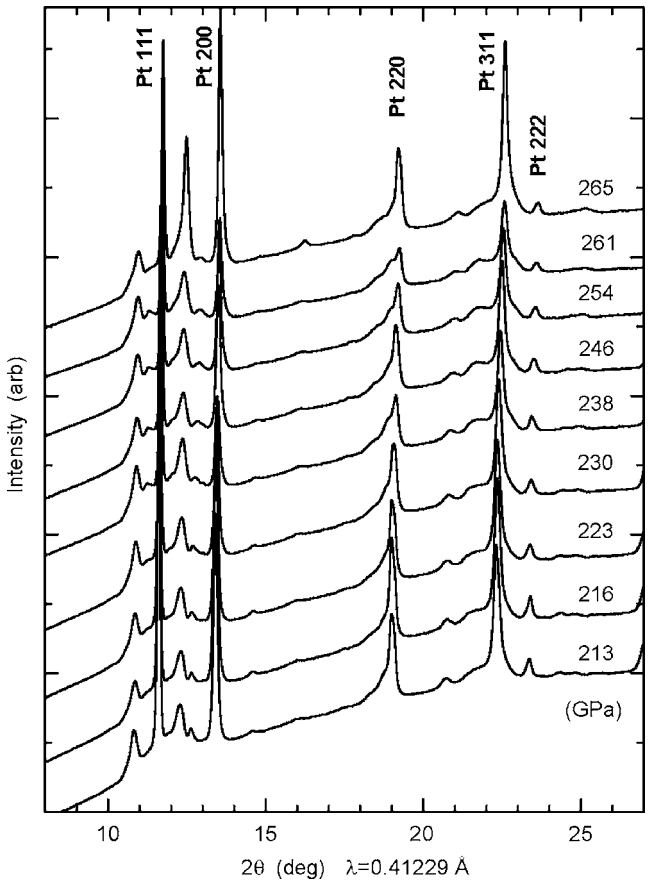

FIG. 2. X-ray diffraction patterns of *c*-Pt-B recorded with a beveled-anvil diamond cell at SPring8. The Pt peaks are labeled and all other peaks are from the Re gasket.

microstresses vary randomly in direction and magnitude in each crystallite[46] and produce microstrains that cause the diffraction lines to broaden. The product of linewidth due to microstrains and Young's modulus is also a measure of the compressive yield strength of the sample material.[17–19,47–49]

II. EXPERIMENTAL DETAILS

The coarse-grained sample of platinum (*c*-Pt-A, 99.99% purity) and the nanocrystalline sample of platinum (*n*-Pt, 99.9% purity) were obtained from Goodfellow Corporation, Pennsylvania, USA and Sigma-Aldrich Co., Missouri, USA, respectively. The average grain sizes of the samples, as determined from the linewidth analysis of high-resolution diffractometer patterns, were 300(20) and 20(3) nm for *c*-Pt and *n*-Pt, respectively. The experiments with *c*-Pt-A carried out at HPCAT used DAC with flat anvil faces (300 μm). Stainless steel gaskets (90 μm central holes) were used to contain the sample. No pressure transmitting medium was used as the objective was to maximize the nonhydrostatic stresses in the sample. The pressure was increased in steps of ~5 GPa, and the diffraction patterns were recorded on an image plate at each pressure using primary x-ray beam of 0.036 81 nm wavelength, collimated to a cross section of 10×10 μm^2 full width at half maximum (FWHM). The first five or six diffraction lines could be recorded (Fig. 1). The maximum pressure reached was 64 GPa. The diffraction experiments on *n*-Pt were carried out using a DAC with *c*-BN seats for the diamond anvils. This design of the DAC permitted full diffraction rings to be recorded. The dimensions of the anvil faces and the gaskets were same as those in the experiments with *c*-Pt-A samples. The maximum pressure reached in the experiments with *n*-Pt samples was 70 GPa. Typical patterns are shown in Fig. 1. The experiments carried out at SPring8, Hyogo, Japan, used beveled anvils with flat faces of 30 μm diameter. The platinum samples (*c*-Pt-B, grain size of ~300 nm) in the form of foil were contained in Re gaskets and the x-ray beam diameter was 10 μm. Since several sets of data were gathered over a period of time, the available wavelengths at the time of experiments were 0.041 229, 0.032 976, and 0.032 751 5 nm. The diffraction patterns recorded in a typical experiment are shown in Fig. 2. The highest pressure reached in these experiments was 330 GPa. Further details of the experiments with beveled anvils can be found in the earlier publications.[3,4] The pressures in all the runs were determined using the measured volume compression of Pt in the equation of state proposed by Holmes *et al.*[6] The four-parameter pseudo-Voigt function with a linear background term (a total of six adjustable parameters) was fitted to the intensity-2θ data of each diffraction peak, and the width (FWHM) and peak position were determined.

III. METHOD OF DATA ANALYSIS

A. Linewidth analysis

The width of a powder diffraction line (hkl) is related to the grain size and microstrain by[46,50]

$$(2w_{hkl}\cos\theta_{hkl})^2 = (\lambda/D)^2 + \langle\eta\rangle^2\sin^2\theta_{hkl}. \quad (1)$$

This form applies to the angle-dispersive powder diffraction data. The terms θ_{hkl}, $2w_{hkl}$, λ, $\langle\eta\rangle$, and D denote, respectively, the diffraction (Bragg) angle, FWHM on $2\theta_{hkl}$ scale,

wavelength of x rays, average microstrain in the crystallites, and the grain size. A detailed discussion on the use of Eq. (1) in the width analysis of the high-pressure diffraction patterns can be found in earlier studies.[17–19,49] The analysis of the diffraction linewidths recorded in the energy dispersive mode can be found elsewhere.[15,47,48,51] The $(2w_{hkl}\cos\theta_{hkl})^2$ versus $\sin^2\theta_{hkl}$ plot is a straight line. The grain size D and $\langle\eta\rangle$ can be determined from the intercept and slope of the line, respectively. The compressive strength is given by

$$\sigma_Y(w) = \langle\eta\rangle E/2. \tag{2}$$

Here, $\sigma_Y(w)$ denotes the compressive strength determined from the linewidth analysis and E is Young's modulus of the polycrystalline aggregate at high pressure. Knowing the pressure-dependent bulk modulus K and shear modulus G of the aggregate, E can be computed from the relation

$$E = 9GK/(3K+G). \tag{3}$$

B. Line-shift analysis

The lattice parameter $a_m(hkl)$ for the cubic system measured under nonhydrostatic stress condition with conventional geometry wherein the primary x-ray beam passes parallel to load axis of the DAC is given by[11,13,31]

$$a_m(hkl) = M_0 + M_1[3(1-3\sin^2\theta_{hkl})\Gamma(hkl)], \tag{4}$$

$$M_0 = a_P\{1+(\alpha t/3)(1-3\sin^2\theta_{hkl})\times[(S_{11}-S_{12}) - (1-\alpha^{-1})(2G_V)^{-1}]\}, \tag{5a}$$

$$M_1 = -a_P\alpha t S/3, \tag{5b}$$

$$\Gamma(hkl) = (h^2k^2+k^2l^2+l^2h^2)/(h^2+k^2+l^2)^2, \tag{5c}$$

$$S = S_{11}-S_{12}-S_{44}/2, \tag{5d}$$

$$\alpha t \cong -3M_1/SM_0. \tag{6}$$

Here, a_P is the lattice parameter at a hydrostatic pressure $(2\sigma_1+\sigma_3)/3$, S_{ij} are the single-crystal elastic compliances, and $t=(\sigma_3-\sigma_1)=\sigma_Y(s)$ is the compressive strength determined from the line-shift analysis. The parameter α describes the true stress state across the boundaries separating the crystallites in a polycrystalline aggregate. The values $\alpha=0$ and $\alpha=1$ denote the conditions of strain and stress continuities across the crystallite boundaries, respectively. To a good approximation, the $a_m(hkl)$ versus $3(1-3\sin^2\theta)\Gamma(hkl)$ plot (gamma plot) is a straight line with M_0 and M_1 as the intercept and slope, respectively. Equation (6) can be used to determine $\sigma_Y(s)$. The S_{ij} required in Eq. (6) are at high pressure. These are derived from the single-crystal elastic moduli C_{ij} at high pressure, which can be obtained using the Birch extrapolation formulation,[52]

$$C_{ij} = C_{ij}(0)x^{5/3}\left\{1+\tfrac{1}{2}[3K(0)C'_{ij}(0)/C_{ij}(0)-5](x^{2/3}-1)\right\}. \tag{7}$$

The symbol (0) denotes the quantity at zero (ambient) pressure. The prime indicates the first pressure derivative and $x=V(0)/V$, where V is the unit cell volume under pressure. The ambient pressure single-crystal moduli and their pressure derivatives are often available from the ultrasonic-velocity measurements. Equation (7) is also valid for the aggregate elastic moduli K and G that are required to compute E from Eq. (3). It may be noted that the ultrasonic technique gives the adiabatic C_{ij}, whereas the isothermal elastic moduli are relevant to the static pressure measurements. The isothermal K is derived by dividing the adiabatic K by a term $(1+\alpha_V\gamma T)$, where α_V, γ, and T are the coefficient of volume expansion, Gruneissen gamma, and temperature in Kelvin, respectively. The quantities G and S are invariant under adiabatic to isothermal conversion. The explicit knowledge of S_{ij} and α is required only when attempt is made to determine t from the diffraction data obtained with the conventional geometry. As discussed in earlier studies,[12–16,34–44] only the shear modulus of the aggregate as function of pressures is required to determine t if the radial diffraction data covering the range $0\leq\psi\leq\pi/2$ are available. Here, ψ denotes the angle between the load axis of the DAC and the diffraction vector. Equation (4) is valid for both angle and an energy dispersive mode of diffraction-data recording, so long as the primary beam passes parallel to the load axis (conventional geometry). In the case of energy dispersive mode, $\theta_{hkl}=\theta_0$, a constant, for all reflections. A slightly modified form of Eq. (4) was used to estimate the compressive strength of Au as a function of pressure from the energy dispersive diffraction data on Au–Zr mixture compressed in a DAC.[53]

It can be easily shown from Eq. (4) that the hydrostatic component of volume compression x_P is related to the measured volume compression x_m by

$$x_P = x_m(1+\beta)^3 \tag{8a}$$

$$\beta = (\alpha t/3)\langle(1-3\sin^2\theta)\rangle\times[S_{11}-S_{12}-3S\langle\Gamma(hkl)\rangle - (1-\alpha^{-1})(2G_V)^{-1}], \tag{8b}$$

$$x_P = V_0/V_P = (a_0/a_P)^3, \tag{8c}$$

$$x_m = V_0/V_m = [a_0/\langle a_m(hkl)\rangle]^3. \tag{8d}$$

The symbol $\langle\rangle$ indicates the average value derived from the observed reflections. It is readily seen that $x_P > x_m$. Thus the pressure computed using the compression x_P is greater than that using x_m. For a given material, the magnitude of the correction factor β depends on the number of reflections used to compute $\langle a_m(hkl)\rangle$. For solids with a positive S, β for the reflections of the type $(h00)$ is larger than that for the reflections of the type (hhh).

The earlier studies on MgO,[17] Fe,[18] and Au (Ref. 19) and W (Ref. 15) show that the strengths derived from the line-shift and linewidth analyses are equal within the experimental error suggesting the following empirical relation:

$$\sigma_Y = \sigma_Y(w) \cong \sigma_Y(s). \tag{9}$$

Here, σ_Y denotes the yield strength under pressure. Assuming the validity of the equality given by Eq. (9), Eqs. (2) and (6) give

$$\alpha \cong [-3M_1/SM_0]/\sigma_Y(w). \tag{10}$$

TABLE I. The single-crystal elastic moduli (isothermal, except those marked adiabatic) and pressure derivative of Pt at ambient pressure from different sources and the derived aggregate properties. Moduli in GPa and S in $(\text{GPa})^{-1}$.

$C_{11}(0)$ $C'_{11}(0)$	$C_{12}(0)$ $C'_{12}(0)$	$C_{44}(0)$ $C'_{44}(0)$	$S(0)$	$G(0)$ $G'(0)$	$K(0)$ $K'(0)$	Method	Ref.
346.7[a]	250.7[a]	76.5	0.003 88	63.5	277	Ultrasonic	54
…	…	…	…	…	…		
338[a]	261.7[a]	72.6	0.006 22	56.1[b]	274	Ultrasonic	55
…	…	…	…	…	…		
…	…	73.243 1.6257	…	…	…	Ultrasonic	56
351.2 6.782(6)	257.5 5.51(2)	73.07 1.927(4)	0.003 83 …	61[b] 1.25[b]	289[c] 5.94[c] 281[d] 5.61[d]	Calculation	9
…	…	…	⋮	63.7 1.6	…	Polycr.-ultrasonic	57
…	…	…	⋮	…	266 5.81	shock wave calculation	6
…	…	…	⋮	…	280 …	Piston cyl.	59

[a]Adiabatic constants.
[b]Voigt–Reuss–Hill average (Ref. 58).
[c]The values obtained when Eq. (7) is fitted to the $(C_{11}+2C_{12})/3$ versus x data obtained from the first-principles calculations (Ref. 9).
[d]The values obtained by fitting Vinet equation to the pressure-volume data from first-principles calculations (Ref. 9).

C. Elasticity data

The elastic moduli of Pt from various sources are listed in Table I. The single-crystal elastic moduli measured by ultrasonic technique by MacFarlane *et al.*,[54] Collard and McLellan,[55] and the data on $C_{44}(0)$ and $C'_{44}(0)$ from the measurements by Biswas *et al.*[56] are compared in Table I. The first-principles calculations of the single-crystal elastic moduli as a function of pressure to 650 GPa have been carried out recently using density functional theory.[9] The Birch extrapolation formula given by Eq. (7) fits the computed $C_{ij}-x$ data very well. The $C_{ij}(0)$ and $C'_{ij}(0)$ obtained from these fits with standard errors are also listed in Table I. The maximum spread in the elastic moduli from different sources is ~5%. Though the magnitude of such differences appears small, these introduce large differences in the values of $S(0)$. For example, the S-values derived from the data MacFarlane *et al.*[54] and Collard and McLellan[55] differ by 45%. The $S(0)$-value from the $C_{ij}(0)$ from the first-principles calculations[9] agrees well with that obtained from the data of MacFarlane *et al.*[54] Though the $C_{44}(0)$-values from the first-principles calculations[9] and the measurements by Biswas *et al.*[56] agree well, the $C'_{44}(0)$-values differ significantly. The measured $G(0)$ of the polycrystalline aggrgate[57] is in reasonable agreement with those computed under Voigt–Reuss–Hill scheme[58] from the $C_{ij}(0)$ data of MacFarlane *et al.*[53] and of Menéndez-Proupin and Singh.[9] However, the measured $G'(0)$ (Ref. 57) is significantly larger than that obtained from the first-principles calculations.[9] No measurements of $C'_{11}(0)$ and $C'_{12}(0)$ are available in the literature. The isothermal bulk modulus $K(0)$ from direct volume-compression measurements by Bridgman[59] is in good agreement with those from other measurements and first-principles calculations. The values of $K(0)=289$ GPa and $K'(0)=5.94$ are obtained by fitting Eq. (7) to the computed[9] $(C_{11}+2C_{12})/3$ versus x data. The corresponding K-P data are marked K_{I} in Fig. 3. A set of values, $K(0)=281$ GPa and $K'(0)=5.61$, is obtained by fitting Vinet equation of state[60] to the pressure-volume data obtained from the first-principles calculations.[9] An expression for K in terms of x was derived by differentiating the Vinet equation with respect to x. The K-x data were computed from this equation using $K(0)=281$ GPa and $K'(0)=5.61$, and converted to K-P data. This set is close to the K_{I}-set and not shown in Fig. 3 for clarity. The K-P data

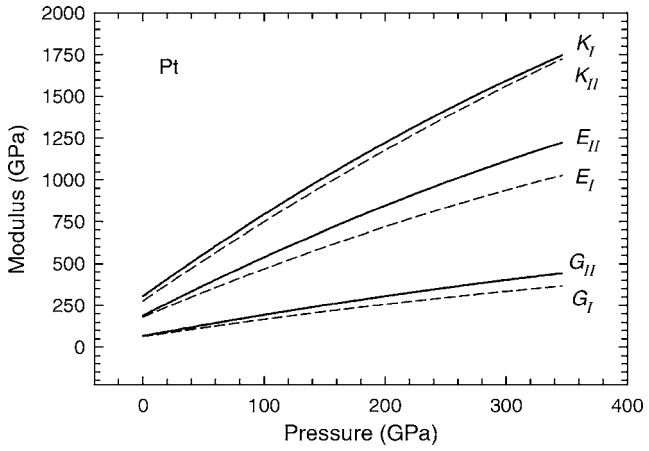

FIG. 3. Pressure dependences of bulk (K), shear (G), and Young's (E) moduli from different sources. Subscript I denotes data from Ref. 9; K_{II}-computed from data in Ref. 6; G_{II}-computed from data in Ref. 57; E_{II}-computed using K_{I} and G_{II}.

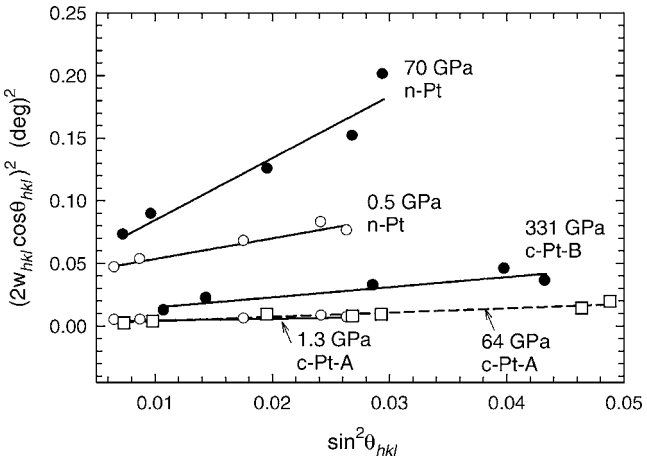

FIG. 4. Typical $(2w_{hkl}\cos\theta_{hkl})^2$ vs $\sin^2\theta_{hkl}$ plots.

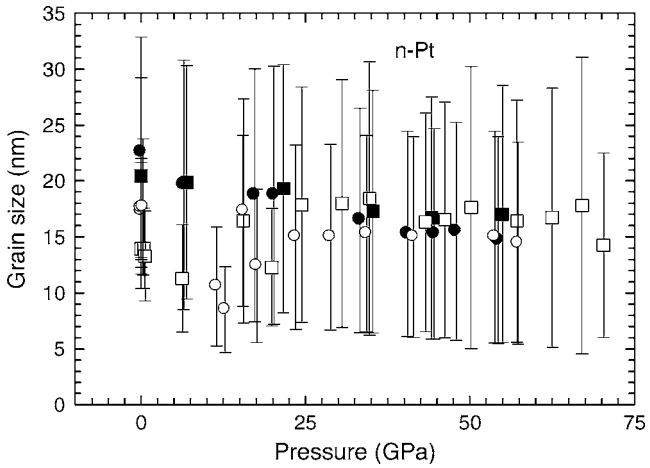

FIG. 5. Grain sizes of *n*-Pt as a function of pressure from two different runs are shown by circles and squares. Unfilled symbols: increasing pressure; filled symbols: decreasing pressure.

derived from the equation of state suggested by Holmes *et al.*[6] are marked K_{II} in Fig. 3. The difference between K_I and K_{II} is ~8% in the low pressure region and decreases to ~2% at 350 GPa. The K_I-P data are used in Eq. (3) to compute E-P data. Two sets of G-x data were computed from Eq. (7) using $G(0)$ and $G'(0)$ obtained from the first-principles calculations[9] and those from the experiments,[57] and the corresponding G-P data are marked G_I and G_{II}, respectively, in Fig. 3. The difference between G_I and G_{II} is ~4% at zero pressure and increases to ~16% at 350 GPa. Similar magnitude of difference is seen in E_I-P and E_{II}-P data computed with G_I-P and G_{II}-P, respectively. We use E_{II}-P data for analyzing the linewidths. The parameter S derived from the first-principles calculations[9] decreases smoothly from 0.0038 GPa^{-1} at zero pressure to 0.0016 GPa^{-1} at 350 GPa.

IV. RESULTS AND DISCUSSION

A. Grain size and strength from linewidths

The $(2w_{hkl}\cos\theta_{hkl})^2$ versus $\sin^2\theta_{hkl}$ plots were constructed for each pressure run using the measured linewidths. A few such plots are shown in Fig. 4. The standard errors in the intercepts obtained from these plots were much larger than the estimated intercepts for the grain sizes of order of 300 nm. The correction for the instrumental broadening[18,19] resulted in negative intercepts in many cases. The grain sizes computed in the remaining cases exhibited large spread. Because of this reason, the pressure dependence of grain size of *c*-Pt could not be determined. The grain size of *n*-Pt sample could be determined with greater certainty because of the small grain sizes that resulted in large intercepts. Figure 5 shows that grain size decreases on initial loading and then increases and becomes nearly pressure independent at higher pressures. The decreasing pressure data show clearly a steady increase of grain size from 14(3) nm at 70 GPa to 20(3) nm at zero pressure. This is reminiscent of the reversible grain-size reduction under pressure observed in an earlier study on *n*-Au.[19] The reversibility indicates that the grains in *n*-Pt samples do not comminute under pressure. The reduction, however, is too large to be explained on the basis of pure compressibility effect. We are unable to offer any satisfactory explanation for the reversible grain-size reduction under pressure.

The strengths of *c*-Pt and *n*-Pt as function of pressure are shown in Fig. 6. Both *c*-Pt-A and *c*-Pt-B samples exhibit comparable strengths. The strength increases linearly from 0.2 GPa at 0 GPa to 4 GPa at 115 GPa. The data show a 0.5 GPa drop in strength at 115 GPa. Though the magnitude of this drop is within the errors of measurement, this feature persists in two independent runs on *c*-Pt-B. The origin of this feature is not clear. Beyond 115 GPa, the strength again increases linearly and reaches 10 GPa at 330. If the feature at 115 GPa is ignored, then the strength of *c*-Pt shows a linear dependence on pressure according to the relation

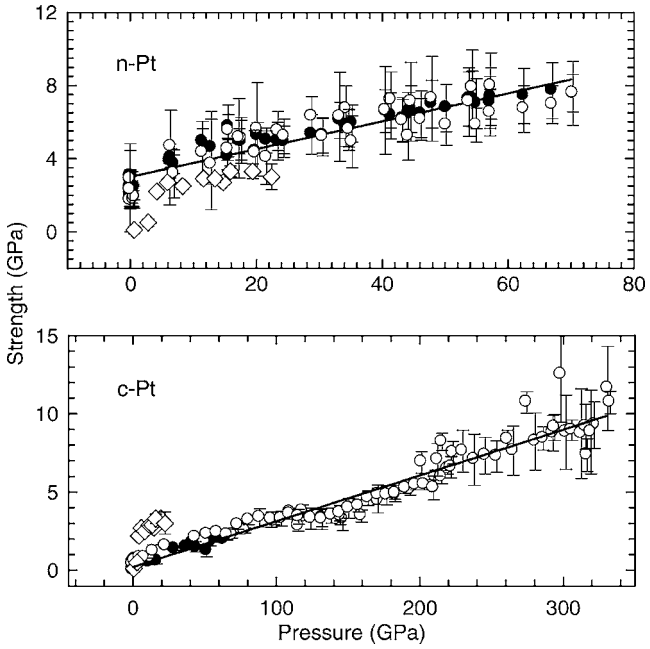

FIG. 6. Strength as a function of pressure. *c*-Pt from Eq. (2): filled circles: sample-A, unfilled circles: sample-B. *n*-Pt: filled circles: from Eq. (2), unfilled circles: from Eq. (6), diamonds: data from Ref. 16

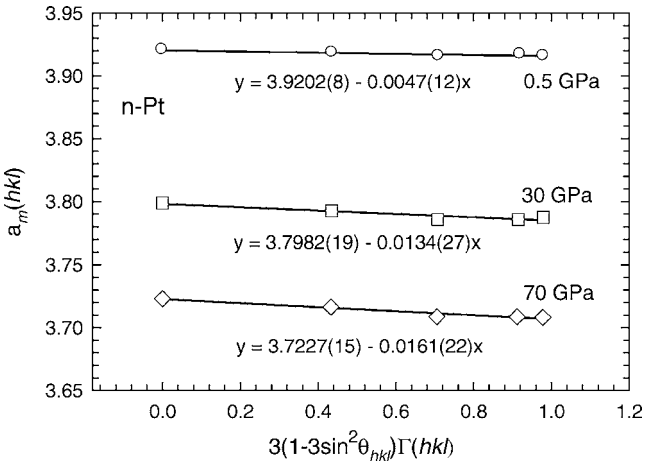

FIG. 7. Typical gamma plots for *n*-Pt. $a_m(hkl)$ is in angstrom units.

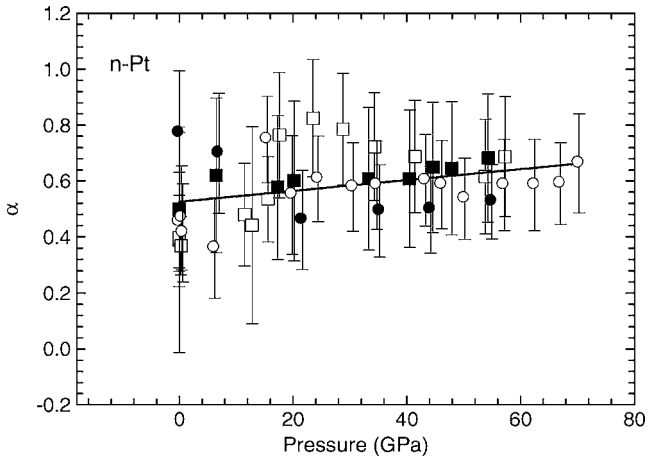

FIG. 8. Pressure dependence of α derived from Eq. (10) for *n*-Pt.

$$\sigma_Y = \sigma_Y(w) = 0.21(2) + 0.029(1)P. \quad (11)$$

Here, P is pressure in gigapascals. The tensile strength of Pt at ambient pressure is reported to be in the range of 0.124–0.165 GPa for the samples annealed at 700 °C and 0.207–0.241 GPa for the cold worked samples.[61] Since the samples compressed in the DAC undergo plastic deformation (cold working), the zero pressure strength derived in the present measurement is within the range of strengths obtained on cold worked samples in standard tensile tests. The strength of *n*-Pt is much larger than that of *c*-Pt (Fig. 6). The strength increases from 3.0(1) to 8.0(3) GPa as the pressure increases from 0 to 70 GPa. These results confirm the findings of earlier high-pressure studies[17,19] that the smaller grain-size sample exhibits higher strength. The grain-size dependence of strength at ambient pressure is well known.[62–64] The strength data of Pt derived from the radial x-ray diffraction by Kavner and Duffy[16] are also shown in Fig. 6. Though not designed to study the grain-size effect on strength, Kavner and Duffy[16] used Pt samples in two different forms, powder of stated grain size of ~1 μm and Pt foil of unspecified grain size. The strength for such large grained samples should be close to the present data on *c*-Pt. As expected, the strengths at pressures below 3 GPa reported by Kavner and Duffy[16] lie close to the present data for *c*-Pt. However, the strength increases steeply with increasing pressure and, in the 15–22 GPa pressure range, becomes comparable to the strength of *n*-Pt obtained in the present study. Without the information on the actual grain sizes, the strength data obtained by Kavner and Duffy[16] cannot be critically compared with the present results. It may be noted that the material suppliers often state the particle size of the powder samples. It is important to distinguish the particle size from the grain size, as a particle generally is an agglomerate of several crystallites. The grain size of the sample should be measured by electron microscopy or diffraction linewidth analysis while comparing the strength data on different samples.

B. Strength from line shifts

The gamma plots for *n*-Pt data show the straight-line trend predicted by Eq. (4) with small scatter. Typical gamma plots are shown in Fig. 7. The estimation of t requires the knowledge of α, which under high pressure is expected to lie between 0.5 and 1. In the early studies,[26,29] α=1 was used to derive the lower bound of strength. While extracting elastic constants of Au from diffraction data under nonhydrostatic compression, it was noticed that high-pressure C_{44}-values were in better agreement with the extrapolated values using ultrasonic elasticity data if α=0.5 was assumed.[14] In earlier studies,[19,45] the strength estimated using Eq. (2) agreed well with that obtained from Eq. (6) with α=0.5. Even in the present case, Eq. (6) with α=0.5 gives $\sigma_Y(s)$-values that are in good agreement with the corresponding $\sigma_Y(w)$-values obtained from Eq. (2). We derive α using Eq. (9) to get the best match between $\sigma_Y(s)$ and $\sigma_Y(w)$, and also to examine the pressure dependence of α. The α-P data [Fig. 8] show large scatter about an average value of 0.6(1). A feeble straight-line trend is seen with 0.002(1) and 0.53(3) as the slope and intercept, respectively. Considering the facts that S is extremely sensitive to the errors in C_{ij} and Eq. (9) represents only an empirical relation, the slope of the straight line seen in the α-P plot is physically not significant. The t-values obtained with α=0.6 are shown in Fig. 6. The strength of *n*-Pt from combined $\sigma_Y(w)$ and $\sigma_Y(s)$ versus pressure data is given by the relation

$$\sigma_Y = 3.0(1) + 0.076(4)P. \quad (12)$$

The straight-line fits to gamma plots with data on *c*-Pt-A and *c*-Pt-B samples gave very low R^2-values in most cases. In the case of *c*-Pt-A, only two runs gave R^2=0.9 and resulted in good values of t. Many runs showed the expected negative slope of the line, but because of poor linear correlation the standard errors in t were inordinately large. Equation (5b) suggests that the slope of the gamma plot for a given material depends on the magnitude of αSt. It is seen from Fig. 9 that the value of αSt for *c*-Pt at any pressure is much smaller than that for *n*-Pt. The limit of smallest αSt that can be measured from the slope of the gamma plot essentially depends on the precision of the measurement of d-spacings. The results suggest that the values of αSt for *c*-Pt shown in Fig. 9 represent the limit of detection with the present day precision of d-spacing measurement. An extreme case arises when the diffraction data from a polycrystalline aggregate containing elastically isotropic crystals are exam-

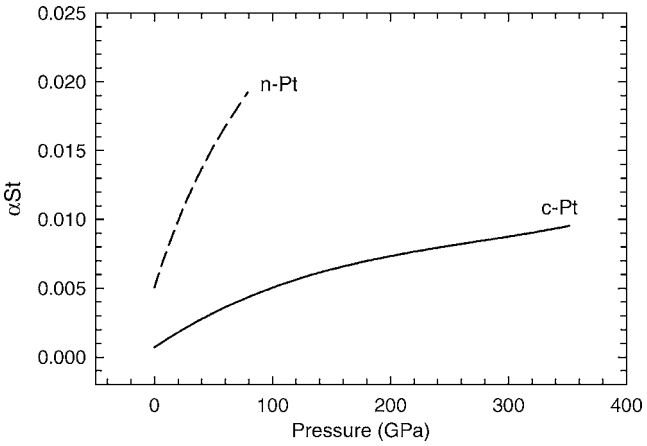

FIG. 9. The αSt vs P plot with α=0.6 and t computed from Eq. (12).

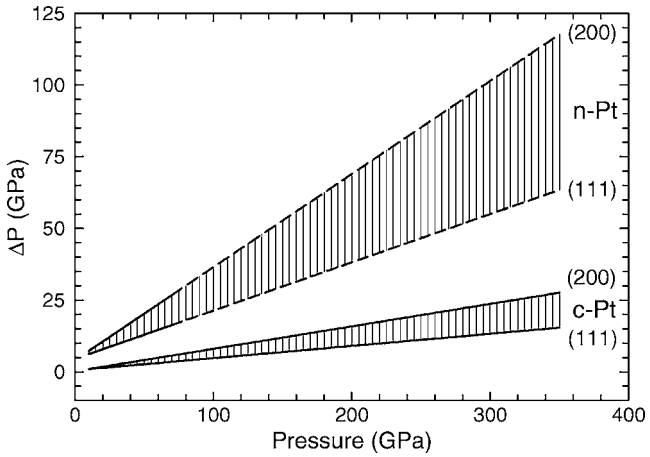

FIG. 10. The pressure correction ΔP for nonhydrostatic compression effect in Pt as a function of pressure. The solid and dashed lines show pressure corrections based on measured and extrapolated strengths, respectively.

ined. Since S=0 in this case, the slope of the gamma plot vanishes and Eq. (6) cannot be used to estimate strength. This limitation applies only to the analysis of the line-shift data taken with the conventional geometry of the DAC. The radial diffraction data have no such limitation. A more detailed discussion of this aspect can be found elsewhere.[20]

The Young's modulus and anisotropy parameter S derived from the single-crystal elasticity data have been used in the present analysis. The use of such data for n-Pt implies the assumption that the single-crystal elastic moduli do not change on reducing the crystallite size of Pt to ~20 nm. A number of studies support this assumption. The measurements of Young's modulus on low-porosity compacts of nanocrystalline Cu and Pd showed only a small decrease from the value for coarse-grained samples.[64] This decrease was attributed to the presence of residual porosity in the samples. The high-pressure x-ray diffraction measurements and the first-principles calculations on nanocrystalline nickel showed no significant difference between the bulk moduli of nanosized and large grained nickel.[65] The experiments on iron samples of 10 nm grain size yielded bulk modulus close to that of large grained samples.[66] In a more recent x-ray diffraction study under hydrostatic pressure, the measured bulk modulus of SiC of 30 nm grain size was in agreement with that of large-grained sample.[67] The first-principles atomistic calculations of the elastic properties of metallic face-centered-cubic nanocrystals show that the material length scale for elasticity is small.[68] Estimates using this analysis suggest that the size effect on elasticity for Pt becomes important only at grain sizes below ~5 nm. These results justify the use of single-crystal elasticity data for the analysis of diffraction patterns of n-Pt in this study.

C. Pressure correction

A set of x_m-values was chosen in 0–330 GPa pressure range. The corresponding x_P values were calculated using the relation given by Eq. (8a). The required values of t at different pressures were computed from Eqs. (11) and (12) for c-Pt and n-Pt, respectively, and a value of 0.6 was taken for α. The differences ΔP between the pressures computed using x_P and x_m are shown in Fig. 10. Since S is positive for Pt, the ΔP versus P plots for the reflections (111) and (200) represent the lower and upper bounds, respectively. For c-Pt, ΔP increases from 0 to 15 GPa for (111) and from 0 to 26 GPa for (200) as the pressure increases from 0 to 330 GPa. For n-Pt, ΔP increases from 0 to 16 GPa for (111) and from 0 to 27 GPa for (200) as pressure increases from 0 to 70 GPa. If the linear increase of strength of n-Pt given by Eq. (12) is assumed to be valid to higher pressures then the values of ΔP at 330 GPa for (111) and (200) are 60 and 110 GPa, respectively. The value of ΔP computed using $\langle x_m \rangle$ with any number of reflections lies in the hatched region.

V. CONCLUSIONS

The strength of coarse-grained platinum is found to increase linearly from 0.2 GPa at zero pressure to 10 GPa at a pressure of 330 GPa. The strength of nanocrystalline platinum sample (20 nm grain size) is much higher than that of coarse-grained sample. It increases linearly from 3 to 8 GPa as the pressure is increased from 0 to 70 GPa and extrapolates to 28 GPa at 330 GPa. The pressures computed from the x-ray measured volume compressions under nonhydrostatic compression are underestimated. In case the coarse-grained platinum is used a pressure marker, the pressure correction is zero at zero pressure and at 330 GPa it increases to a value that lies between 15 and 26 GPa depending on the reflections used to compute the average volume compression. The pressure correction is nearly fourfold larger if platinum of 20 nm grain size is used as pressure marker. Often platinum powder of unspecified grain size is used as a pressure marker. The grain-size dependence of strength and resulting effect on the pressure correction should be kept in mind while using platinum as a pressure standard in x-ray diffraction experiments.

[1]H. K. Mao, Y. Wu, L. C. Chen, J. F. Shu, and A. P. Jephcoat, J. Geophys. Res. **95**, 21737 (1990).
[2]D. Andrault, G. Fiquet, F. Guyot, and M. Hanfland, Science **282**, 720 (1998).
[3]Y. Akahama, H. Kawamura, and A. K. Singh, J. Appl. Phys. **92**, 5892 (2002).
[4]Y. Akahama, M. Nishimura, K. Kinoshita, and H. Kawamura, Phys. Rev. Lett. **96**, 045505 (2006).
[5]R. G. McQueen, S. P. Marsh, J. W. Taylor, J. M. Fritz, and W. J. Carter, in

High Velocity Impact Phenomena, edited by R. Kinslow (Academic, New York, 1970), pp. 293 and 530.
[6]N. C. Holmes, J. A. Moriarty, G. R. Gathers, and W. J. Nellis, J. Appl. Phys. **66**, 2962 (1989).
[7]Y. Wang, R. Ahuja, and B. Johannson, J. Appl. Phys. **92**, 6616 (2002).
[8]S. Xiang, L. Cai, Y. Bi, and F. Jing, Phys. Rev. B **72**, 184102 (2005).
[9]E. Menéndez-Proupin and A. K. Singh, Phys. Rev. B **76**, 054117 (2007).
[10]A. K. Singh, High Temp. - High Press. **10**, 641 (1978).
[11]A. K. Singh, J. Appl. Phys. **73**, 4278 (1993); **74**, 5920 (1993).
[12]A. K. Singh, H. K. Mao, J. Shu, and R. J. Hemley, Phys. Rev. Lett. **80**, 2157 (1998).
[13]A. K. Singh, C. Balasingh, H. K. Mao, R. J. Hemley, and J. Shu, J. Appl. Phys. **83**, 7567 (1998).
[14]T. S. Duffy, G. Shen, J. Shu, H. K. Mao, R. J. Hemley, and A. K. Singh, J. Appl. Phys. **86**, 6729 (1999).
[15]D. He and T. S. Duffy, Phys. Rev. B **73**, 134106 (2006).
[16]A. Kavner and T. S. Duffy, Phys. Rev. B **68**, 144101 (2003).
[17]A. K. Singh, H. P. Liermann, and S. K. Saxena, Solid State Commun. **132**, 795 (2004).
[18]A. K. Singh, A. Jain, H. P. Liermann, and S. K. Saxena, J. Phys. Chem. Solids **67**, 2197 (2006).
[19]A. K. Singh, H. P. Liermann, S. K. Saxena, H. K. Mao, and S. Usha Devi, J. Phys.: Condens. Matter **18**, S969 (2006).
[20]A. K. Singh, J. Phys. Chem. Solids **65**, 1589 (2004).
[21]A. L. Ruoff, J. Appl. Phys. **46**, 1389 (1975).
[22]A. K. Singh and G. C. Kennedy, J. Appl. Phys. **45**, 4686 (1974).
[23]T. Uchida, N. Funamori, and T. Yagi, J. Appl. Phys. **80**, 739 (1996).
[24]C. J. Howard and E. H. Kisi, J. Appl. Crystallogr. **32**, 624 (1999).
[25]S. Matthies, H. G. Priesmeyer, and M. R. Daymond, J. Appl. Crystallogr. **34**, 585 (2001).
[26]A. K. Singh and G. C. Kennedy, J. Appl. Phys. **47**, 3337 (1976).
[27]G. L. Kinsland and W. A. Bassett, Rev. Sci. Instrum. **47**, 130 (1976).
[28]G. L. Kinsland and W. A. Bassett, J. Appl. Phys. **48**, 978 (1977).
[29]T. S. Duffy, H. K. Mao, and R. J. Hemley, Phys. Rev. Lett. **74**, 1371 (1995).
[30]R. J. Hemley, H. K. Mao, G. Shen, J. Badro, P. Gllet, M. Hanfland, and D. Häusermann, Science **276**, 1242 (1997).
[31]A. K. Singh and K. Takemura, J. Appl. Phys. **90**, 3269 (2001).
[32]K. Takemura and A. K. Singh, Phys. Rev. B **73**, 224119 (2006).
[33]S. Usha Devi and A. K. Singh, Physica B & C **138 & 140**, 922 (1986).
[34]H. K. Mao, J. F. Shu, G. Y. Shen, R. J. Hemley, B. Li, and A. K. Singh, Nature (London) **396**, 741 (1998).
[35]T. S. Duffy, G. Shen, D. L. Heinz, Y. Ma, J. Shu, H. K. Mao, R. J. Hemley, and A. K. Singh, Phys. Rev. B **60**, 15063 (1999).
[36]S. R. Shieh, T. S. Duffy, and B. Li, Phys. Rev. Lett. **89**, 255507 (2002).
[37]S. R. Shieh, T. S. Duffy, and G. Shen, Phys. Earth Planet. Inter. **143–144**, 93 (2004).
[38]S. Speziale and T. S. Duffy, Phys. Chem. Miner. **29**, 465 (2002).
[39]S. Merkel, H. R. Wenk, J. Shu, G. Shen, P. Gillet, and R. J. Hemley, J. Geophys. Res. **107**, 2217 (2002).
[40]S. Merkel, A. P. Jephcoat, J. Shu, H. K. Mao, P. Gillet, and R. J. Hemley, Phys. Chem. Miner. **29**, 1 (2002).
[41]F. Jiang, S. Speziale, S. R. Shieh, and T. S. Duffy, J. Phys.: Condens. Matter **16**, S1041 (2004).
[42]D. W. He, S. R. Shieh, and T. S. Duffy, Phys. Rev. B **70**, 184121 (2004).
[43]S. Merkel, J. Shu, P. Gillet, H. K. Mao, and R. J. Hemley, J. Geophys. Res. **110**, B05201 (2005).
[44]B. Kiefer, S. R. Shieh, T. S. Duffy, and T. Sekine, Phys. Rev. B **72**, 014102 (2005).
[45]A. K. Singh, E. Menéndez-Proupin, G. Gutiérrez, Y. Akahama, and H. Kawamura, J. Phys. Chem. Solids **67**, 2192 (2006).
[46]A. R. Stokes and A. J. C. Wilson, Proc. Phys. Soc. London **56**, 174 (1944).
[47]D. J. Weidner, Y. Wang, and M. T. Vaughan, Science **266**, 419 (1994).
[48]J. Chen, D. J. Weidner, and M. T. Vaughan, Nature (London) **419**, 824 (2002).
[49]A. K. Singh, H. P. Liermann, Y. Akahama, and H. Kawamura, J. Appl. Phys. **101**, 123526 (2007).
[50]J. I. Langford, J. Appl. Crystallogr. **4**, 164 (1971).
[51]L. Gerward, S. Morup, and H. Topsoe, J. Appl. Phys. **47**, 822 (1976).
[52]F. Birch, J. Geophys. Res. **83**, 1257 (1978).
[53]A. K. Singh, K. Vijayan, H. Xia, Y. K. Vohra, and A. L. Ruoff, *Recent Trends in High Pressure Research: Proceeding of the 13th AIRAPT-International Conference on High pressure Science and Technology*, 1991 edited by Anil K. Singh (Oxford IBH, New Delhi, (1992).
[54]R. E. Macfarlane, J. A. Rayne, and C. K. Jones, Phys. Lett. **18**, 91 (1965).
[55]S. M. Collard and R. B. McLellan, Acta Metall. Mater. **40**, 699 (1992).
[56]S. N. Biswas, M. J. P. Muringer, and C. A. Ten Seldam, Phys. Status Solidi A **141**, 361 (1994).
[57]M. Guinan and D. Steinberg, J. Phys. Chem. Solids **35**, 1501 (1974).
[58]R. Hill, Proc. Phys. Soc., London, Sect. A **65**, 349 (1952).
[59]P. W. Bridgman, Proc. Am. Acad. Arts Sci. **74**, 11 (1940).
[60]P. Vinet, J. Ferranti, J. H. Rose, and J. R. Smith, J. Geophys. Res. **92**, 9319 (1987).
[61]W. H. Cubberly, H. Baker, D. Benjamin, P. M. Unterweisser, C. W. Kirkpatrick, V. Knoll, and K. Nieman, *Metal Handbook*, 9th edition (American Society for Metals, Metals Park, OH, 1979), Vol. 2, p. 688.
[62]E. O. Hall, Proc. Phys. Soc. London, Sect. B **64**, 747 (1951).
[63]N. J. Petch, J. Iron Steel Inst., London **174**, 25 (1953).
[64]P. G. Sanders, J. A. Eastman, and J. R. Weertman, Acta Mater. **45**, 4019 (1997).
[65]S. Rekhi, S. K. Saxena, R. Ahuja, B. Johansson, and J. Hu, J. Mater. Sci. **36**, 4719 (2001).
[66]B. Chen, D. Penwell, M. B. Kruger, A. F. Yue, and B. Fultz, J. Appl. Phys. **89**, 4794 (2001).
[67]H. Liu, J. Hu, J. Shu, D. Häusermann, and H.-K. Mao, Appl. Phys. Lett. **85**, 1973 (2004).
[68]V. B. Shenoy, Phys. Rev. B **71**, 094104 (2005).